frontiers | Frontiers in Marine Science

TYPE Original Research
PUBLISHED 20 September 2024
DOI 10.3389/fmars.2024.1428621

OPEN ACCESS

EDITED BY
Jun Zhao,
Ministry of Natural Resources, China

REVIEWED BY
Ruifeng Zhang,
Shanghai Jiao Tong University, China
Cunde Xiao,
Beijing Normal University, China

*CORRESPONDENCE
Jeremy D. Owens
jdowens@fsu.edu

RECEIVED 06 May 2024
ACCEPTED 26 July 2024
PUBLISHED 20 September 2024

CITATION
Kenlee B, Owens JD, Raiswell R, Poulton SW, Severmann S, Sadler PM and Lyons TW (2024) Long-range transport of dust enhances oceanic iron bioavailability.
Front. Mar. Sci. 11:1428621.
doi: 10.3389/fmars.2024.1428621

Long-range transport of dust enhances oceanic iron bioavailability

Bridget Kenlee[1], Jeremy D. Owens[2]*, Robert Raiswell[3], Simon W. Poulton[3], Silke Severmann[4], Peter M. Sadler[1] and Timothy W. Lyons[1]

[1]Department of Earth and Planetary Sciences, University of California, Riverside, Riverside, CA, United States, [2]Department of Earth, Ocean & Atmospheric Science, Florida State University National High Magnetic Field Laboratory, Tallahassee, FL, United States, [3]School of Earth and Environment, University of Leeds, Leeds, United Kingdom, [4]Department of Marine and Coastal Sciences, Rutgers University, New Brunswick, NJ, United States

Wind-borne dust supply of iron (Fe) to the oceans plays a crucial role in Earth's biogeochemical cycles. Iron, a limiting micronutrient for phytoplankton growth, is fundamental in regulating ocean primary productivity and in turn the global carbon cycle. The flux of bioavailable Fe to the open ocean affects oscillations in atmospheric CO_2 due to its control on inorganic carbon fixation into organic matter that is eventually exported to the sediments. However, the nature of dust-delivered Fe to the ocean and controls on its bioavailability remain poorly constrained. To evaluate the supply of wind-borne bioavailable Fe and its potential impact on Fe-based climate feedbacks over the last 120,000 years, we examine sediment profiles from four localities that define a proximal to distal transect relative to Saharan dust inputs. Bulk δ^{56}Fe isotope compositions (average = -0.05‰) and Fe_T/Al ratios suggest crustal values, thus pointing to a dominant dust origin for the sediments at all four sites. We observed no variability in grain size distribution or in bioavailable Fe supply at individual sites as a function of glacial-versus-interglacial deposition. Importantly, there is no correlation between sediment grain size and Fe bioavailability. Spatial trends do, however, suggest increasing Fe bioavailability with increasing distance of atmospheric transport, and our sediments also indicate the loss of this Fe and thus potential bioavailability utilization once deposited in the ocean. Our study underscores the significance of Fe dynamics in oceanic environments using refined speciation techniques to elucidate patterns in Fe reactivity. Such insights are crucial for understanding nutrient availability and productivity in various ocean regions, including the Southern Ocean, where wind-delivered Fe may play a pivotal role. It is expected that dust delivery on glacial-interglacial timescales would be more pronounced in these high-latitude regions. Our findings suggest that studies linking Fe availability to marine productivity should benefit significantly from refined Fe speciation approaches, which provide insights into the patterns and controls on Fe reactivity, including atmospheric processing. These insights are essential for understanding the impacts on primary production and thus carbon cycling in the oceans and consequences for the atmosphere.

KEYWORDS

iron, dust, isotopes, productivity, glacial-interglacial

1 Introduction

As the dominant source of iron (Fe) to the open oceans (Fung et al., 2000), wind-borne (aeolian) dust is an integral part of Earth's climate system. Iron, an essential micronutrient, plays an important role in regulating the oceanic biological pump due to its limited bioavailability for phytoplankton in large regions of the ocean (Martin and Fitzwater, 1988; Jickells et al., 2005). Consequently, Fe bioavailability exerts a strong control on levels of atmospheric carbon dioxide (CO_2) and climate on global scales (Joos et al., 1991; Baker et al., 2003; Boyd and Ellwood, 2010). North Africa is one of the primary sources of dust to Earth's atmosphere, where it is subsequently deposited in the oceans and on continents (Engelstaedter et al., 2006). Downwind from North Africa, dust-driven fertilization may enhance long-term productivity in Western Atlantic regions including Amazon rain forests and Floridian, Bahamian, and Caribbean coral reefs and water columns (Shinn et al., 2000; Muhs et al., 2007; Bristow et al., 2010; Prospero and Mayol-Bracero, 2013; Swart et al., 2014; Yu et al., 2015). More generally, transport-dependent enhancement of iron bioavailability may have been a factor in determining the loci of primary productivity in the oceans throughout Earth's history.

Importantly, not all dust-borne Fe is bioavailable in the ocean, and the processes that enhance Fe bioavailability are not well understood. Atmospheric deposition of Fe in the open ocean is predominantly via fine-grained iron (oxyhydr)oxide (mostly as grain coatings) and silicate minerals (Raiswell and Canfield, 2012). Previous studies have suggested that the chemical properties of Fe in atmospheric dust are often grain size-dependent (Hand et al., 2004; Baker and Jickells, 2006; Ooki et al., 2009). Furthermore, with longer transport times in the atmosphere, Fe solubility (and consequently Fe bioavailability) should increase via atmospheric processing, principally involving acid production via photochemistry (Hand et al., 2004). The signatures of these processes, however, are yet to be explored systematically in modern sediments using carefully calibrated iron extraction techniques or other chemical fingerprints. Instead, past studies have often characterized potentially soluble iron (Fe_{Sol}) as bioavailable Fe, emphasizing reactive minerals such as ferrihydrite (Wells et al., 1983; Fan et al., 2006). However, ferrihydrite is thermodynamically unstable and will transform into more stable phases on diagenetic timescales, including (oxyhydr)oxides such as goethite, hematite, and magnetite, or other secondary phases such as pyrite and Fe-carbonates. The critical implication is that measured values for the residual, most reactive phases in sediment cores may underestimate the total original reactive Fe pool (Schwertmann et al., 2004).

Here, we have adopted a scheme for iron speciation that is more inclusive of Fe phases that may have been bioavailable prior to transformations in seawater and early lithification. We define a broader array of Fe mineral pools as being highly reactive (Fe_{HR}) because their precursors may have initially been bioavailable. These mineral phases consist of (a) carbonate Fe (plus weakly bound, surface Fe); (b) amorphous and crystalline Fe oxides and (oxyhydr) oxides such as ferrihydrite, goethite, and hematite; (c) magnetite Fe; and (d) pyrite (Poulton and Canfield, 2005). We normalize Fe_{HR} to total Fe (Fe_T) to identify relative enrichments or deficiencies in the Fe_{HR} pool compared to the entire Fe contents. These Fe_{HR}/Fe_T ratios are robust against potential artifacts of dilution (e.g., by carbonate or biogenic silica), which can otherwise obscure interpretations of absolute concentrations. It is important to note that substantial portions of all these phases may have formed by mineral transformation of initially soluble and bioavailable precursor phases following deposition (Benner et al., 2002). Therefore, Fe_{HR} effectively serves as upper limit proxy for the residual concentration of the initial bioavailable Fe (Sur et al., 2015; Sardar Abadi et al., 2020). While this approach may overestimate the original bioavailable Fe pool due to inputs such as detrital magnetite, it provides a comprehensive baseline against which enrichments and depletions in formerly bioavailable forms can be assessed. This approach is conservative, in terms of percentages, because percent loss from Fe_{HR} would be low relative to the loss from the smaller amount of the most soluble original Fe (Fe_{Sol}). However, sediment cores are unlikely to contain significant amounts of these original phases due to expected rapid diagenetic transformations, which contribute to the various Fe_{HR} pools.

Several recent studies have addressed the controls and distribution of recent aeolian bioavailable Fe in the oceans and subsequent climate feedbacks (Lis et al., 2015; Shoenfelt et al., 2018; Thöle et al., 2019), including grain size controls on aerosol Fe solubility (Baker and Jickells, 2006; Mackie et al., 2006; Trapp et al., 2010), but none has focused on characterization, spatial trends, and grain size relationships as preserved in marine sediments over glacial-interglacial cycles. To isolate trends in aeolian bioavailable iron in marine sediments, four sample locations that preserve marine sedimentary records of African dust export were strategically selected from International Ocean Discovery Program sites (IODP or previous iterations of the program—ODP and initial IODP) to provide a wide spatial distribution in the Northern Atlantic Ocean from core repositories (Figure 1) from the last glacial period to present (about the last 120,000 years). We use bulk Fe isotopes to identify the potential end-member sources to these sites. Additionally, we examined grain size characteristics and quantified various Fe pools to assess controls on bioavailable Fe distribution. We document that dust-borne Fe at distal sites experiences enhanced atmospheric processing, leading to an increase in Fe_{Sol}, which was readily available to primary producers (Hassler et al., 2011; Borchardt et al., 2019). Instantaneous consumption of Fe_{Sol} could have stimulated primary productivity. The net effect would be increases in the overall impact with increasing distance from the Saharan source, which may also reduce Fe delivery to the sediments.

2 Material and methods

2.1 Study sites

The four locations studied are sites 658 (21°N, 19°W) and 659 (18° N, 21°W) from ODP expedition 108, located on top of the Cape Verde

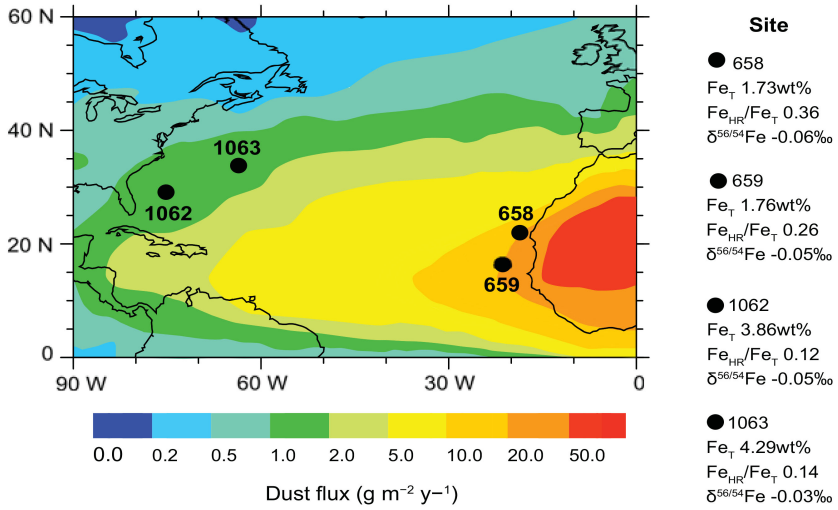

FIGURE 1
Locations of IODP sites 658, 659, 1062 and 1063 with Fe data. Base map shows estimates for dust deposition (g m^{-2} y^{-1}) — specifically transport of African dust across the surface ocean. Dust flux data are from Jickells et al. (2005), Mahowald et al. (1999), and Ginoux et al. (2001); all other data are from this study. Highly reactive Fe (Fe_{HR}) for each site is normalized to total Fe (Fe_T) to distinguish relative enrichments or deficiencies in the Fe_{HR} pool. Also shown are the Fe isotope compositions ($\delta^{56}Fe$) to constrain different sources of Fe.

Plateau near the northwest African continental margin, and sites 1062 (28°N, 74°W) and 1063 (33°N, 57°W) from the sediment drifts of the western North Atlantic Ocean as part of ODP Leg 172. The sites were selected because they span a wide portion of the Northern Atlantic Ocean (Figure 1). The marine sedimentary records of North African dust export offer the advantage of continuous sedimentation (Tiedemann et al., 1989; Giosan et al., 2002). These sites range from proximal to distal relative to the Sahara Dust Corridor source region. The average time resolution of the four records is about 4 kyr/sample covering the last glacial period to present (over the last 120,000 years) (Supporting Information).

2.2 Dust deposition average

Calculations of dust deposition (g m^{-2} y^{-1}) were obtained from the average of three models (Mahowald et al., 1999; Ginoux et al., 2001; Jickells et al., 2005) (Supplementary Table S7) to represent our best approximations of dust delivery.

2.3 Grain size analysis

Grain size distribution (GSD) in marine sediments are often used as a measure of dust delivery (Blott and Pye, 2001; Harrison et al., 2001; Baker et al., 2006; Ooki et al., 2009). Samples were dried at 80°C. Dry sieving was carried out for 15 minutes using a tapping sieve shaker (RO-TAP) equipped with a set of stainless-steel sieves. Short sieving times prevented the formation of aggregates due to electrostatic interactions and interparticle cohesion. Each fraction was weighed and recorded. Particle size distribution is represented graphically using a cumulative distribution curve and the D value method (S. J. Blott and Pye, 2001) from GRADISTAT (Blott, 2000). Samples were divided into >45µm (bulk), 45 to 20µm, and<20µm size fractions.

2.4 Iron speciation and iron isotope analysis

We used a state-of-the-art sequential Fe extraction procedure modified from Poulton and Canfield (2005) to characterize the Fe phases present ($Fe_{Na\text{-}Ac}$, Fe_{Dith}, and Fe_{Ox}), including minerals that might have formed diagenetically from initially bioavailable Fe. All Fe extracts were analyzed by inductively coupled plasma-mass spectrometry (ICP-MS; Agilent 7500ce) with H_2 and He modes in the collision cell, diluted with trace-metal grade 2% HNO_3 to enhance Fe detection by reducing interferences, thereby improving the accuracy of analytical results.

A multi-acid digest was performed to determine total solid-phase iron (Fe_T) and aluminum (Al) concentrations. Dried samples were ashed at 550°C, and a standard three-step digestion was performed using trace metal grade HF, HNO_3, and HCl at 140°C. This way, the potential bioreactivity of the Fe can be expressed as a fraction of the total Fe pool. Final concentrations were determined using the same ICP-MS. Reference standards SDO-1 (Devonian Ohio Shale) and SCO-1 (Cody Shale) were digested and analyzed in parallel with the sample extractions and yielded errors of less than<4%.

Splits from the multi-acid digest were used to measure the Fe isotope composition of the bulk sample ($\delta^{56}Fe_T$). Iron isotopes were analyzed at all four sites, resulting in total of 38 isotopic analyses (Supplementary Table S11) Anion exchange resin and a standard ion chromatography protocol were used for Fe separation to eliminate matrix effects (Skulan et al., 2002; Arnold et al., 2004). Column yields were carefully monitored using the Ferrozine

colorimetric method with UV-Vis spectrophotometry (λ = 562 nm) (Viollier et al., 2000) before and after chromatographic purification, ensuring only samples with yields ≥95% were used for isotopic analysis. Isotopic compositions were measured on a Neptune Thermo Scientific MC-ICP-MS (Multiple Collector-Inductively Coupled Plasma-Mass Spectrometer) at Rutgers University, applying the method of Arnold et al. (2004). Samples were introduced as a 1 ppm solution using a cyclonic spray chamber. Mass bias during the analysis was corrected using a Cu elemental spike, and standard reference material IRMM-014 served as a bracketing standard between each sample for accurate mass bias correction. The blank procedure involved spiking the blanks post-column separation to prevent overestimation of the procedure blank from incomplete spike recovery, ensuring accurate accounting of any blank contributions and preventing inaccuracies in the final results. The iron isotope composition (δ^{56}Fe) is defined as follows:

$$\delta^{56}\,Fe_{‰} = \left[\frac{(^{56}Fe/^{54}Fe)_{sample}}{(^{56}Fe/^{54}Fe)_{IRMM-14}}\right] - 1\ x\ \ 1,000,$$

where the δ^{56}Fe is reported relative to IRMM-014 reference material. The measured Fe isotope composition of IRMM-014 is $\delta^{56}Fe_T$ =-0.09‰ on this scale, with an internal precision of ±0.06‰ (2σ).

2.5 Carbon concentrations

Sedimentary total carbon (TC) was analyzed by combustion using an Eltra CS-500 carbon-sulfur analyzer. Total inorganic carbon (TIC) was determined by acidification of a split of the sample. Total organic carbon (TOC) content was calculated as the difference between TC and TIC. The Eltra limestone geostandards AR4007 and AR4011 were analyzed routinely, with values falling within reported ranges and deviating less than<5%. Geo-reference standards AR4007 (carbon = 7.58%) and AR4011 (carbon = 8.91%) were used for analytical calibration and quality control. Calcium carbonate concentrations ($CaCO_3$), as weight percent (wt. %), were calculated from the measured TIC content assuming that all evolved CO_2 was derived from the dissolution of $CaCO_3$:

$$CaCO_3(wt.\,\%) = TIC\ x\ 8.33\ (wt.\,\%)$$

Standard $CaCO_3$ (>99.9% calcium carbonate, Fisher Scientific) was used during individual batches of analyses to confirm accuracy and instrument performance before, during, and after each run (with reproducibility better than 3%). No correction was made for the presence of other carbonate minerals.

2.6 Statistical analysis

The analysis of variance (ANOVA), the F-test, and t-tests were conducted to determine whether there is a significant difference of bioavailable Fe distribution between proximal and distal sites and to assess any dependence of Fe_{HR}/Fe_T with grain size (Montgomery et al., 2009; Haynes, 2013). The 95% confidence interval was used in all analyses (see Supplementary Information for grouping rationale and sensitivity analyses).

2.7 Aerosols optical properties

Aerosol optical depth (AOD) data are from the MIRS—Multi-angle Imaging SpectroRadiometer (https://misr.jpl.nasa.gov/getData/accessData/). These data provide a benchmark for calibrating models and interpreting sediment records that span long-term geological timescales. The averaged concentration of AOD between 2009-2019 over the North Atlantic Ocean was utilized to provide an estimate of atmospheric African dust deposition to the North Atlantic Ocean. Modern AOD data help bridge temporal scales, offering historical perspectives on changes in dust patterns and aerosol loading, while sediment cores offer long-term insights into dust deposition and iron (Fe) content over glacial-interglacial cycles.

2.8 The ecoGEnIE model

To model the relationship between Fe flux and primary productivity dynamics, we used the ecoGEnIE paleoclimate model, an extension of cGEnIE—a carbon-centric, Grid Enabled Integrated Earth system model featuring comprehensive marine biogeochemical uptake (Ward et al., 2018). ecoGEnIE incorporates a scheme for plankton ecology (ECOGEM) with a size-dependent control on the plankton biogeochemical function (Ward et al., 2018). This addition allows for a better representation of biodiversity, including ecosystem shifts in response to environmental forcing. ecoGEnIE provides dynamic simulations of nutrient usage in response to availability. For our purposes, we used cGEnIE/ecoGEnIE default configurations (Ridgwell and Hargreaves, 2007).

3 Results and discussion

3.1 Iron supply from the North African dust to the North Atlantic Ocean

Iron isotope data (δ^{56}Fe) can be a powerful way to constrain the Fe sources to the oceans over Earth history (Beard et al., 2003; Waeles et al., 2007; Owens et al., 2012; Conway et al., 2019). The average bulk δ^{56}Fe values for samples from all four sites (-0.05 ± 0.02‰; 2-standard deviations) is consistent with continentally derived dust (Figure 1, Supplementary Table S1) given the similarity to the δ^{56}Fe composition of most silicate rocks (Beard et al., 2003; Dauphas and Rouxel, 2006; Waeles et al., 2007; Conway and John, 2014). The Fe_T/Al ratio of 0.55 ± 0.02 also overlaps with the mean Fe_T/Al ratio for terrigenous sediments and average continental crust (0.55 ± 0.11; Martinez et al., 2007), suggesting no significant hydrothermal contribution, which typically has a δ^{56}Fe similar to crustal values but has a Fe_T/Al >2.00 (Clarkson

et al., 2014; Raiswell et al., 2018a). Our average Al/Ti ratio of 18.9 ± 0.78 is also consistent with an aeolian origin for our samples (Yarincik et al., 2000).

The potential Fe bioavailability can be explored by speciation studies, which are broadly linked to Fe phases in the sample (Shi et al., 2009). The concentrations of Fe extracted using sodium acetate ($Fe_{Na\text{-}Ac}$) comprised 0.5-2.9 wt.% of Fe_T (Supplementary Tables S2a-d, S3a-d). Although Poulton and Canfield (2005) used $Fe_{Na\text{-}Ac}$ to remove carbonate-bound Fe, their data show that minor amounts are also removed from iron-bearing silicates. We confirmed this possibility by extracting a range of Fe-bearing silicates with sodium acetate (Supplementary Table S4), suggesting that acetate removes a minor fraction of Fe from such minerals—potentially from weakly bound surface sites (Heron et al., 1994; Raiswell et al., 2018b). This silicate-associated pool has been documented to be readily bioavailable (Shoenfelt et al., 2017) because Fe(II)-rich silicate minerals can enhance diatom growth as well as photosynthetic efficiency. However, this silicate-bound Fe fraction is very small relative to the other potentially bioavailable pools we now discuss. A dithionite Fe extraction (Fe_{Dith}), dominantly representing Fe (oxyhydr)oxide minerals, removed 8.6 to 21.6 wt.% of Fe_T (Supplementary Tables S2a-d, S3a-d). Previous studies have considered Fe_{Dith} to be an effective measure of potentially bioavailable iron from aeolian dust particles (Fan et al., 2006; Baker and Croot, 2010). An oxalate Fe extraction (Fe_{Ox}) mainly targets Fe in magnetite and ranges from 5.4-12.1 wt.% of Fe_T (Supplementary Tables S2a-d, S3a-d). If delivered unaltered to the ocean, rather than forming during diagenesis, magnetite would likely represent refractory (insoluble) iron in surface seawaters.

On the broadest scales, an overall increase in atmospheric dust deposition occurs during glacial intervals due to an expansion in the source areas (Mahowald et al., 1999) and stronger winds (McGee et al., 2010) that consequently influence the supply of bioavailable Fe to the open ocean. However, at low latitudes, there is no significant glacial-interglacial trend in dust input (Maher et al., 2010). Iron bioavailability in marine systems is linked to complexation with prokaryotic-released organic compounds, such as siderophores, polycarboxylate ligands (Barbeau, 2006; Shaked and Lis, 2012), and saccharides (Hassler et al., 2011). Thus, a fraction of this delivered Fe pool should be bioavailable. Our analyses of Fe_T, Fe_{HR}/Fe_T, and total organic carbon (TOC) at each site have limited to no statistically relevant stratigraphic variation over the last glacial period to the present ($p>0.05$) (Figure 2, Supplementary Tables S10a-d). Further, the TOC contents argue against productivity that is enhanced in one interval relative to the other (glacial versus interglacial). This combination of data suggests that there is little or no temporal variation at low latitudes on glacial-interglacial timescales. Importantly, however, past studies have suggested that downwind locations may be impacted biologically by the enhanced solubility of delivered Fe, such as the Bahamas and Amazon region (Shinn et al., 2000; Muhs et al., 2007; Bristow et al., 2010; Muhs et al., 2012; Prospero and Mayol-Bracero, 2013; Swart et al., 2014; Yu et al., 2015). Consistent with this possibility, our data document a

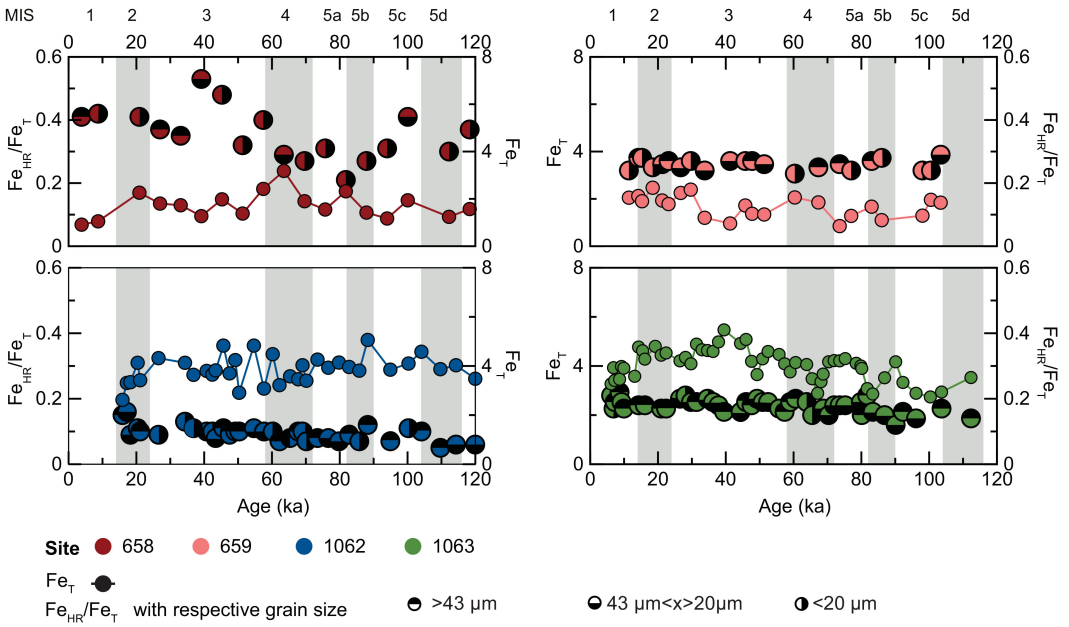

FIGURE 2
Age profiles for iron (Fe) in IODP cores 658 (red), 659 (orange), 1062 (blue), and 1063 (green) showing glacial-interglacial relationships. Gray bars indicate climatic events of importance for the Last Glacial Period (extending back ~ 120,000 years) as recorded in polar ice cores. MIS refers to marine isotope stages. Total Fe (Fe_T) is shown as filled, connected circles for each site. Highly reactive (Fe_{HR}) consists of carbonate Fe (plus weakly bound surface Fe); amorphous and crystalline Fe oxides and (oxyhydr)oxides such as ferrihydrite, goethite, and hematite; and magnetite Fe. Fe_{HR} data are normalized to total Fe (Fe_T) to distinguish relative enrichments or deficiencies in the Fe_{HR} pool. FeHR/Fe_T ratios are expressed in terms of grain size populations.

transport-dependent process that would also be relevant to other regions, such as the south Atlantic, and time intervals that are characterized by Fe limitation. Moreover, our data suggest atmospheric pathways to enhanced reactivity that are relatively constant, at least at low latitude, under glacial versus interglacial global climatic regimes (see discussions below). The glacial-interglacial uniformity we observe implies consistency in sourcing and processing during transport despite temporal differences in weathering relationships in the source regions and wind patterns, among other varying controls (McGee et al., 2013). Additional work is necessary to demonstrate whether the observed relationship is the same for all source regions and latitudes. Importantly, however, this surprising result is likely to influence future climate models for this region and potentially beyond.

3.2 Downcore Fe geochemistry and grain size distribution

The bioavailable Fe supply in sediments as a function of grain size distribution (GSD) during glacial-interglacial periods could have important impacts on marine primary productivity (Mahowald et al., 2014). Therefore, we determined the GSD at all four sites by dry sieving (Supplementary Figure S1, Supplementary Table S5). A statistical one sample t-Test was carried out for all four sites to test the variability of GSD during glacial and interglacial periods, (n=128; Figure 2 and Supplementary Table S9). The p-values for proximal sites 658 and 659 are 0.88 and 0.76, respectively, and 0.72 and 0.19 for distal sites 1062 and 1063, respectively. The end member p-values suggest that variability in GSD over glacial-interglacial timescale is not statistically significant for any of the four sites, consistent with previous findings that the flux of low-latitude Saharan dust does not vary significantly over these timescales (Maher et al., 2010; Skonieczny et al., 2019).

Previous work has suggested that Fe bioavailability is grain size-dependent, primarily due to the greater surface-area-to-volume relationship of small grains of atmospheric dust (Mahowald et al., 2018). Greater relative surface areas for small-sized particles could support proportionally larger surface alteration during transport and associated coatings of soluble Fe. To test for statistically significant differences of bioavailable Fe distribution for GSD in our drill-core sediment samples, Fe_{HR}/Fe_T (n=394) were compared using an analysis of variance (ANOVA) and a t-test (see Supplementary Information for grain size rationale and sensitivity analyses). We found no statistically significant differences in Fe_{HR}/Fe_T with grain size at a given location (Supplementary Tables S8a-d). For example, the ANOVA for site 658 shows no significant dependence ($p<0.05$), with an f-critical value of $2.80e^{-4}$ and a p-value of 1.0 among the various grain sizes. The ANOVA data for site 659 have an f-critical value of 1.13 and a p-value of 0.33, which is also not significant at $p<0.05$. Sites 1062 and 1063 also show no significant dependence at $p<0.05$, with f-critical values of 1.12 and 0.99 and p-values of 0.33 and 0.37 for sites 1062 and 1063, respectively. The negligible variability in potentially bioavailable Fe distribution as a function of GSD in these sediments from each site is likely due, at least in part, to the particles having experienced many series of aggregation and disaggregation as they settled through the water column (Bacon et al., 1985)—thus the larger particles in the sediments are mostly aggregates of finer original materials (Anderson et al., 2016) but initially were larger but through disaggregation and then aggregation have been modified. Consistent with the possibility, our the Fe_{HR}/Fe_T ratios of larger grains are similar to those of smaller particles i.e. showing no significant locality relation between GSD and Fe geochemistry (Supplementary Figure S3). Importantly, the results from these cores do not suggest there is a statistical difference in grain size variations related to in Fe reactivity among grains of differing primary size.

3.3 Spatial trends in potentially bioavailable Fe distribution

North African dust is carried great distances over thousands of kilometers, as would be true for any ocean basin. Because atmospheric transport is a size-selective process (Pye, 1989), proximal and distal Fe dust can be distinguished by the grain-size distributions related to distance from the source, whereby dust particle size decreases with increasing distance (Mahowald et al., 2014). Average particle size distributions for our samples show a decrease of ~20% in grain size (Supplementary Table S5) and a corresponding increase of ~30% in surface area (Supplementary Table S6) from proximal to distal sites. Small particles have a longer lifetime in the atmosphere and thus experience enhanced atmospheric processing (chemical and/or photochemical), likely leading to an increase in the solubility (Fe_{Sol}) of Fe_{HR} (Spokes et al., 1994; Desboeufs et al., 2001; Shi et al., 2009). This suggests these grains are disaggregated primary grains where the finer distal grains (as suggested by grain size analyses) have traveled farther - increasing processing time. Thus, these finer distal grains have high surface are-to-volume ratios, which also favors the extent of processing.

Our measurements show a systematic decrease in Fe_{HR}/Fe_T from proximal to distal sites (Figure 3A). Importantly, suggestions of lower total Fe concentrations at proximal sites (Figure 3B) mostly reflect increased carbonate dilution at those locations. Detailed insight into Fe behavior is provided by our Fe_{Dith} data, which show the greatest decrease, from 21.5 wt.% and 15.5 wt.% of Fe_T at proximal sites 658 and 659, respectively, to 9.0 wt.% at both distal sites (1062 and 1063; Supplementary Tables S2a-d and S3a-d). We suggest that our Fe_{HR}/Fe_T ratios decrease with increasing transport due to enhanced Fe solubility via atmospheric reactions (Oakes et al., 2012), leading to dissolution in seawater and likely uptake of the bioavailable Fe by primary producers in the surface ocean at these distal sites. Bioavailable Fe delivery and utilization from primary producers has been observed in this general region of the Atlantic previously (Borchardt et al., 2019) and has been suggested for transport of Fe to oligotrophic lakes in Spain (Bhattachan et al., 2016). Modern dust transport from the Saharan desert to the Atlantic shows seasonal differences. In the boreal summer, the trade winds typically carry dust from northern Africa to the Caribbean, while in winter, transport shifts south toward the

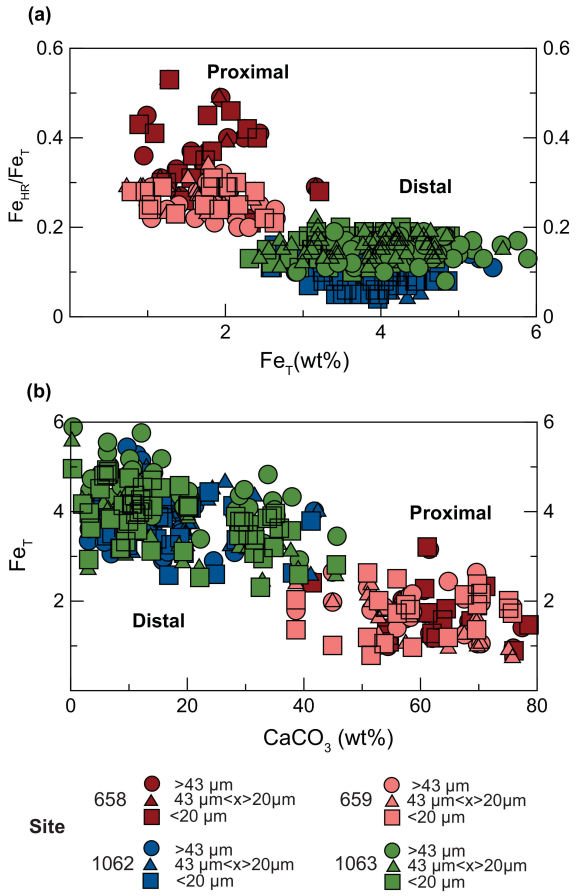

FIGURE 3
(A) Fe_{HR}/Fe_T versus Fe_T for proximal (658-red and 659-orange) and distal (1062-blue and 1063-green) sites. Note the systematic decrease in Fe_{HR}/Fe_T from proximal to distal sites. **(B)** Fe_T versus $CaCO_3$ for proximal and distal sites. The effects of carbonate dilution on Fe_T are confirmed by a steep inverse relationship between Fe_T and $CaCO_3$ content across all sites and in all size fractions. Samples with grain size >45µm (bulk), 45 to 20µm, and<20µm are shown as a circles, triangles, and squares, respectively. There is no significant difference in Fe_{HR}/Fe_T among the grain size populations from a given site.

Amazon Basin (Bakker et al., 2019). This relationship indicates that the central and western Sahara are significant dust sources in the productive summer, while the Sahel region contributes more dust to the Caribbean during the winter. (Figure 4A). Furthermore, the aerosol optical depth (AOD) decreases progressively from the Sahara Desert to the open ocean. Continued research on seasonal dust transport variation is crucial for a comprehensive understanding of these dynamics and the seasonal impacts, particularly since these may evolve due to climate change. The ecoGEnIe model suggests significant increases in Fe flux (Figure 4B) in these distal locations, underscoring the significant role of dust deposition. This scenario, based on limited data, is thought provoking and highlights an area of research that should be explored. Evaluating our experiments, we confirm that lower Fe concentrations may indeed reflect higher carbonate dilution in these specific locations. However, full quantification of the loss of soluble Fe and the role of transport in Fe bioavailability will require more information about the North African dust source region (Huneeus et al., 2011; McGee et al., 2013), post-depositional processing of the Fe (Bressac and Guieu, 2013; Meskhidze et al., 2019), biogeochemical conditions of the surface seawater (Boyd and Ellwood, 2010), and atmospheric processes (Baker and Croot, 2010).

Further, it is important to consider alternative interpretations of our data. For example, the Fe content of analyzed dust samples could decrease downwind of North Africa, as described by Zhang et al. (2015), due to selective, progressive loss of heavier hematite-rich grains through gravitational settling during transport in the atmosphere. In truth, many of our observations are consistent with this possibility, and it may play a role, but there are other observations that are less consistent. First, it is not clear that the trend observed in Fe deposition in Zhang et al. (2015) is an expression of hematite availability. Other Fe phases, in particular Fe (oxyhydr)oxides, are likely a substantial part of the Fe pool in the dust—both as original constitutes from the source region and as products of atmospheric reactions. Importantly, these phases are approximately half as dense as crystalline hematite and would be decidedly less vulnerable to differential settling effects during transport. Moreover, soil hematite, the likely source of dust, would also be less dense than well-crystallized hematite, and these Fe phases are likely to be only a small part of the total grain mass (discrete Fe oxide grains are rare; Poulton and Raiswell, 2005). Further, hematite and other Fe(III) phases are often present as coatings on aluminosilicate grains that tend, if anything, to have lower densities than other silicates.

Our detailed speciation provides additional insight. Specifically, we see the same distal trends in our data from the acetate extraction, which does not target hematite but instead extracts more reactive, less dense Fe (oxyhydr)oxide phases. Finally, we also do not observe a difference in Fe chemistry as a function of grain size, in contrast to expected transport-related physical sorting that is controlled by grain size and/or density. These observations do not preclude other important processes, but they do leave us with our interpretation as the most parsimonious explanation of the full range of observations.

4 Conclusion

The potential effects of iron fertilization via dust delivery likely scale (although perhaps not linearly) with the total dust input and the proportion of bioavailable (soluble) Fe present. Our results show that while dust fluxes decrease with transport distance, the solubility/bioavailability of the associated iron increases downwind as a consequence of greater transport distance and thus greater time of exposure to atmospheric photochemical reactions that favor transformation to more soluble Fe(III) phases as conceptualized in Figures 5A–F. The decrease in Fe_{HR}/Fe_T ratios in downwind sediments fingerprints a loss of bioavailable Fe upon deposition due to dissolution. Despite lower dust fluxes compared to upwind sites (Figure 4A),

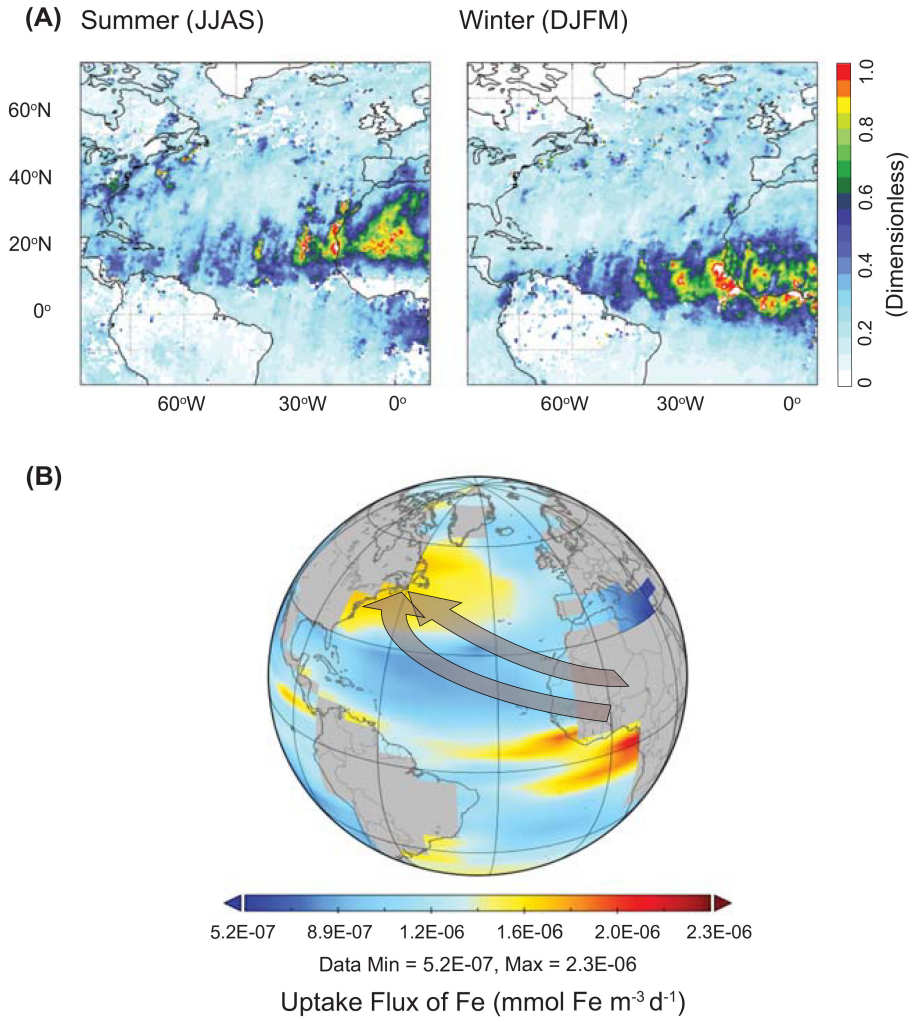

FIGURE 4
(A) Modern dust transport over the North Atlantic Ocean. Map of dust aerosol optical depth (AOD) over the North Atlantic showing the transport of African dust across the North Atlantic Ocean during the boreal summer [June-July-August-September (JJAS)] and boreal winter [December-January-February-March (DJFM)]. AOD is a measure of the extinction of the solar beam by dust and haze. It is a dimensionless number that is related to the amount of aerosol in the vertical column of atmosphere over the observation location. **(B)** Uptake of Fe flux modeled using ecoGEnIE. Gray arrow indicates the African dust that are carried from Northern Africa across the Atlantic Ocean.

our data are consistent with the idea of downwind loci of elevated bioavailability of the iron that stimulated primary productivity (Figure 4B). This enhanced reactivity at distal sites is likely more important than the consequences of more abundant inputs of less-soluble Fe upwind. Previous studies have suggested enhanced biological activity linked to these Fe patterns, including microbial response in the surface layers (Borchardt et al., 2019), nitrogen fixation of the North Atlantic Ocean (Moore et al., 2009), carbonate production in Bahamas (Shinn et al., 2000), growth of the coral reefs in the Caribbean (Swart et al., 2014), and the fertilization of Amazon region (Bristow et al., 2010). For instance, Swart et al. (2014) argued for dust-related stimulation of Fe-limited nitrogen-fixing cyanobacteria in the Bahamas leads to local drawdown of CO_2 and carbonate precipitation.

In summary, distal sites exhibit lower dust fluxes and total Fe delivery but higher reactivity compared to proximal locations that are dominated by relatively insoluble phases (Bhattachan et al., 2016), so that even high total dust fluxes would result in relatively low delivery of bioavailable Fe. In contrast, the distal sites receive less dust, but the Fe is highly soluble and bioavailable because of distance-dependent transport processing in the atmosphere. This Fe, we argue, is lost upon deposition in the ocean, which results in the lower residual ratio of reactive to total iron in the sedimentary record compared to the sediments of the proximal sites. Beyond recent impacts in the North Atlantic, our findings suggest that enhanced of Fe bioavailability at distal sites could help explain patterns of biological activity and organic accumulation relative to dust source in other regions throughout Earth history (Sardar Abadi et al., 2020). Our study emphasizes the significance of exploring Fe speciation to improve our understanding of Fe dynamics across various temporal scales, including glacial-interglacial periods. This

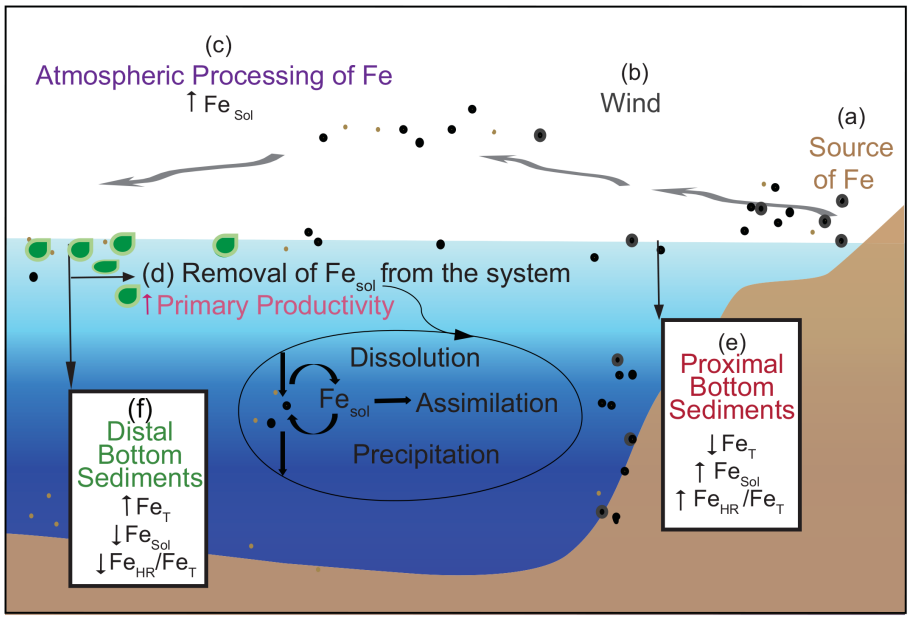

FIGURE 5
Generalized schematic of the iron biogeochemical cycle. The major source of Fe in the open ocean is dust delivered by the atmosphere. Fe_T: total, Fe_{HR}: highly reactive Fe (at least partly bioavailable Fe at the time of deposition), and Fe_{Sol}: soluble Fe (bioavailable Fe that is readily used for primary productivity). **(A)** Source of dust is from the Sahara Desert. **(B)** Wind eroding soils containing Fe oxides and silicates leads to transport of the dust seaward. Coarse particles will sink rapidly, while smaller particles will travel further in the atmosphere and remain in the surface ocean longer. **(C)** Atmospheric processing can increase Fe solubility and bioavailability. **(D)** In the ocean, Fe_{Sol} is removed from the system via dissolution and is assimilated by the phytoplankton. The dissolved Fe does not remain in solution in oxic seawater since oxidation to Fe(III) is rapid, and seawater is close to saturation with iron(oxyhydr)oxides. **(E)** Sediments of proximal sites show relatively low values for Fe_T due to carbonate dissolution and relatively high Fe_{Sol} and Fe_{HR}/Fe_T. **(F)** Sediments at distal sites show decreases of Fe_{Sol} due to its dissolution and removal by primary producers in the surface ocean, leading to low values for Fe_{Sol} and Fe_{HR}/Fe_T in the underlying sediments.

insight contributes significantly to broader understandings of oceanic and atmospheric carbon cycling. Hopefully, similar studies will be undertaken in other regions, particularly in the Southern Ocean, where nutrient availability may be abundant but primary production is constrained by the availability of reactive Fe. These sites would be influenced strongly by dust and processes analogous to those discussed in this study.

Data availability statement

The original contributions presented in the study are included in the article/Supplementary Material. Further inquiries can be directed to the corresponding author.

Author contributions

BK: Conceptualization, Data curation, Formal analysis, Investigation, Methodology, Project administration, Supervision, Validation, Visualization, Writing – original draft. JO: Conceptualization, Formal analysis, Investigation, Methodology, Supervision, Validation, Visualization, Writing – review & editing. RR: Conceptualization, Formal analysis, Methodology, Writing – review & editing. SP: Formal analysis, Methodology, Writing – review & editing. SS: Methodology, Writing – review & editing. PS: Formal analysis, Methodology, Writing – review & editing. TL: Conceptualization, Formal analysis, Funding acquisition, Investigation, Methodology, Resources, Supervision, Validation, Visualization, Writing – review & editing.

Funding

The author(s) declare financial support was received for the research, authorship, and/or publication of this article. This work was supported by grants from the National Science Foundation (EAR-2026926), NASA Exobiology 80NSSC18K1532 and 80NSSC23K0346, and Alfred P. Sloan Foundation FG-2020-13552 (JO). Funding was also provided (TL) through the NASA Astrobiology Institute under Cooperative Agreement No. NNA15BB03A issued through the Science Mission Directorate, NASA Interdisciplinary Consortia for Astrobiology Research (ICAR), and the Geobiology and Low-Temperature Geochemistry Program of the National Science Foundation.

Conflict of interest

The authors declare that the research was conducted in the absence of any commercial or financial relationships that could be construed as a potential conflict of interest.

The author(s) declared that they were an editorial board member of Frontiers, at the time of submission. This had no impact on the peer review process and the final decision.

Publisher's note

All claims expressed in this article are solely those of the authors and do not necessarily represent those of their affiliated organizations, or those of the publisher, the editors and the reviewers. Any product that may be evaluated in this article, or claim that may be made by its manufacturer, is not guaranteed or endorsed by the publisher.

Supplementary material

The Supplementary Material for this article can be found online at: https://www.frontiersin.org/articles/10.3389/fmars.2024.1428621/full#supplementary-material

References

Anderson, R., Cheng, H., Edwards, R., Fleisher, M., Hayes, C., Huang, K.-F., et al. (2016). How well can we quantify dust deposition to the ocean? *Philos. Trans. R. Soc. A: Mathematical Phys. Eng. Sci.* 374, 20150285.

Arnold, G. L., Weyer, S., and Anbar, A. (2004). Fe isotope variations in natural materials measured using high mass resolution multiple collector ICPMS. *Analytical Chem.* 76, 322–327. doi: 10.1021/ac034601v

Bacon, M. P., Huh, C.-A., Fleer, A. P., and Deuser, W. G. (1985). Seasonality in the flux of natural radionuclides and plutonium in the deep Sargasso Sea. *Deep Sea Res. Part A. Oceanographic Res. Papers* 32, 273–286. doi: 10.1016/0198-0149(85)90079-2

Baker, A. R., and Croot, P. L. (2010). Atmospheric and marine controls on aerosol iron solubility in seawater. *Mar. Chem.* 120, 4–13. doi: 10.1016/j.marchem.2008.09.003

Baker, A. R., and Jickells, T. D. (2006). Mineral particle size as a control on aerosol iron solubility. *Geophysical Res. Lett.* 33(17). doi: 10.1029/2006GL026557

Baker, A. R., Jickells, T. D., Witt, M., and Linge, K. L. (2006). Trends in the solubility of iron, aluminium, manganese and phosphorus in aerosol collected over the Atlantic Ocean. *Mar. Chem.* 98, 43–58. doi: 10.1016/j.marchem.2005.06.004

Baker, A. R., Kelly, S. D., Biswas, K. F., Witt, M., and Jickells, T. D. (2003). Atmospheric deposition of nutrients to the Atlantic Ocean. *Geophysical Res. Lett.* 30 (24). doi: 10.1029/2003GL018518

Bakker, N., Drake, N., and Bristow, C. S. (2019). Evaluating the relative importance of northern African mineral dust sources using remote sensing. *Atmospheric Chem. Phys.* 19, 10525–10535. doi: 10.5194/acp-19-10525-2019

Barbeau, K. (2006). Photochemistry of organic iron(III) complexing ligands in oceanic systems. *Photochem. Photobiol.* 82, 1505–1516. doi: 10.1562/2006-06-16-IR-935

Beard, B. L., Johnson, C. M., Skulan, J. L., Nealson, K. H., Cox, L., and Sun, H. (2003a). Application of Fe isotopes to tracing the geochemical and biological cycling of Fe. *Chem. Geol.* 195, 87–117. doi: 10.1016/S0009-2541(02)00390-X

Beard, B. L., Johnson, C. M., Von Damm, K. L., and Poulson, R. L. (2003b). Iron isotope constraints on Fe cycling and mass balance in oxygenated Earth oceans. *Geology* 31, 629–632. doi: 10.1130/0091-7613(2003)031<0629:IICOFC>2.0.CO;2

Benner, S. G., Hansel, C. M., Wielinga, B. W., Barber, T. M., and Fendorf, S. (2002). Reductive dissolution and biomineralization of iron hydroxide under dynamic flow conditions. *Environ. Sci. Technol.* 36, 1705–1711. doi: 10.1021/es0156441

Bhattachan, A., Reche, I., and D'Odorico, P. (2016). Soluble ferrous iron (Fe (II)) enrichment in airborne dust. *J. Geophysical Res.: Atmospheres* 121, 10–153. doi: 10.1002/2016JD025025

Blott, S. (2000). Grain size distribution and statistics package for the analysis of unconsolidated sediments by sieving or by laser granulometer. *Grandistat* 26, 1237–1248.

Blott, S. J., and Pye, K. (2001). GRADISTAT: A grain size distribution and statistics package for the analysis of unconsolidated sediments. *Earth Surface Processes Landforms* 26(11):1237–1248. doi: 10.1002/esp.261

Borchardt, T., Fisher, K. V., Ebling, A. M., Westrich, J. R., Xian, P., Holmes, C. D., et al (2019). Saharan dust deposition initiates successional patterns among marine microbes in the Western Atlantic. *Limnol. Oceanogr.* 65(1):191-203. doi: 10.1002/lno.11291

Boyd, P., and Ellwood, M. (2010). The biogeochemical cycle of iron in the ocean. *Nat. Geosci.* 3, 675. doi: 10.1038/ngeo964

Bressac, M., and Guieu, C. (2013). Post-depositional processes: What really happens to new atmospheric iron in the ocean's surface? *Global biogeochemical cycles* 27, 859–870. doi: 10.1002/gbc.20076

Bristow, C. S., Hudson-Edwards, K. A., and Chappell, A. (2010). Fertilizing the Amazon and equatorial Atlantic with West African dust. *Geophysical Res. Lett.* 37(14). doi: 10.1029/2010GL043486

Clarkson, M., Poulton, S., Guilbaud, R., and Wood, R. (2014). Assessing the utility of Fe/Al and Fe-speciation to record water column redox conditions in carbonate-rich sediments. *Chem. Geol.* 382, 111–122. doi: 10.1016/j.chemgeo.2014.05.031

Conway, T. M., Hamilton, D. S., Shelley, R. U., Aguilar-Islas, A. M., Landing, W. M., Mahowald, N. M., et al. (2019). Tracing and constraining anthropogenic aerosol iron fluxes to the North Atlantic Ocean using iron isotopes. *Nat. Commun.* 10, 2628. doi: 10.1038/s41467-019-10279-w

Conway, T. M., and John, S. G. (2014). Quantification of dissolved iron sources to the North Atlantic Ocean. *Nature* 511, 212. doi: 10.1038/nature13482

Dauphas, N., and Rouxel, O. (2006). Mass spectrometry and natural variations of iron isotopes. *Mass Spectrometry Rev.* 25, 515–550. doi: 10.1002/mas.20078

Desboeufs, K., Losno, R., and Colin, J.-L. (2001). Factors influencing aerosol solubility during cloud processes. *Atmospheric Environ.* 35, 3529–3537. doi: 10.1016/S1352-2310(00)00472-6

Engelstaedter, S., Tegen, I., and Washington, R. (2006). North African dust emissions and transport. *Earth-Sci. Rev.* 79, 73–100. doi: 10.1016/j.earscirev.2006.06.004

Fan, S.-M., Moxim, W. J., and Levy, H. (2006). Aeolian input of bioavailable iron to the ocean. *Geophysical Res. Lett.* 33(7). doi: 10.1029/2005GL024852

Fung, I. Y., Meyn, S. K., Tegen, I., Doney, S. C., John, J., and Bishop, J. (2000). Iron supply and demand in the upper ocean (vol 14, pg 281, 2000). *Global biogeochemical cycles* 14, 697–700. doi: 10.1029/2000gb900001

Ginoux, P., Chin, M., Tegen, I., Prospero, J., Holben, B., Dubovik, O., et al. (2001). Global simulation of dust in the troposphere: Model description and assessment. *J. Geophys. Res.* 106, 255–220.

Giosan, L., Flood, R. D., Grützner, J., and Mudie, P. (2002). Paleoceanographic significance of sediment color on western North Atlantic drifts: II. Late Pliocene–Pleistocene sedimentation. *Mar. Geol.* 189, 43–61. doi: 10.1016/S0025-3227(02)00322-5

Hand, J. L., Mahowald, N. M., Chen, Y., Siefert, R. L., Luo, C., Subramaniam, A., et al. (2004). Estimates of atmospheric-processed soluble iron from observations and a global mineral aerosol model: Biogeochemical implications. *J. Geophysical Research-Atmospheres* 109(D17). doi: 10.1029/2004JD004574

Harrison, S. P., Kohfeld, K. E., Roelandt, C., and Claquin, T. (2001). The role of dust in climate changes today, at the last glacial maximum and in the future. *Earth-Sci. Rev.* 54, 43–80. doi: 10.1016/S0012-8252(01)00041-1

Hassler, C. S., Schoemann, V., Nichols, C. M., Butler, E. C. V., and Boyd, P. W. (2011). Saccharides enhance iron bioavailability to Southern Ocean phytoplankton. *Proc. Natl. Acad. Sci. United States America* 108, 1076–1081. doi: 10.1073/pnas.1010963108

Haynes, W. (2013). "Student's t-test," in *Encyclopedia of Systems Biology* (New York, NY: Springer), 2023–2025.

Heron, G., Crouzet, C., Bourg, A. C., and Christensen, T. H. (1994). Speciation of Fe (II) and Fe (III) in contaminated aquifer sediments using chemical extraction techniques. *Environ. Sci. Technol.* 28, 1698–1705. doi: 10.1021/es00058a023

Huneeus, N., Schulz, M., Balkanski, Y., Griesfeller, J., Prospero, M., Kinne, S., et al. (2011). Global dust model intercomparison in AeroCom phase I. *Atmospheric Chem. Phys.* 11, 7781–7816. doi: 10.5194/acp-11-7781-2011

Jickells, T. D., An, Z. S., Andersen, K. K., Baker, A. R., Bergametti, G., Brooks, N., et al. (2005). Global iron connections between desert dust, ocean biogeochemistry, and climate. *Science* 308, 67–71. doi: 10.1126/science.1105959

Joos, F., Sarmiento, J. L., and Siegenthaler, U. (1991). Estimates of the effect of Southern Ocean iron fertilization on atmospheric CO2 concentrations. *Nature* 349, 772. doi: 10.1038/349772a0

Lis, H., Shaked, Y., Kranzler, C., Keren, N., and Morel, F. M. (2015). Iron bioavailability to phytoplankton: an empirical approach. *ISME J.* 9, 1003. doi: 10.1038/ismej.2014.199

Mackie, D., Peat, J., McTainsh, G., Boyd, P., and Hunter, K. (2006). Soil abrasion and eolian dust production: Implications for iron partitioning and solubility. *Geochem. Geophys. Geosystems* 7(12). doi: 10.1029/2006GC001404

Maher, B., Prospero, J., Mackie, D., Gaiero, D., Hesse, P. P., and Balkanski, Y. (2010). Global connections between aeolian dust, climate and ocean biogeochemistry at the present day and at the last glacial maximum. *Earth-Sci. Rev.* 99, 61–97. doi: 10.1016/j.earscirev.2009.12.001

Mahowald, N., Albani, S., Kok, J. F., Engelstaeder, S., Scanza, R., Ward, D. S., et al. (2014). The size distribution of desert dust aerosols and its impact on the Earth system. *Aeolian Res.* 15, 53–71. doi: 10.1016/j.aeolia.2013.09.002

Mahowald, N. M., Hamilton, D. S., Mackey, K. R., Moore, J. K., Baker, A. R., Scanza, R. A., et al. (2018). Aerosol trace metal leaching and impacts on marine microorganisms. *Nat. Commun.* 9, 1–15. doi: 10.1038/s41467-018-04970-7

Mahowald, N., Kohfeld, K., Hansson, M., Balkanski, Y., Harrison, S. P., Prentice, I. C., et al. (1999). Dust sources and deposition during the last glacial maximum and current climate: A comparison of model results with paleodata from ice cores and marine sediments. *J. Geophysical Research-Atmospheres* 104, 15895–15916. doi: 10.1029/1999JD900084

Martin, J. H., and Fitzwater, S. E. (1988). Iron deficiency limits phytoplankton growth in the north-east Pacific subarctic. *Nature* 331, 341. doi: 10.1038/331341a0

Martinez, N. C., Murray, R., Thunell, R. C., Peterson, L. C., Muller-Karger, F., Astor, Y., et al. (2007). Modern climate forcing of terrigenous deposition in the tropics (Cariaco Basin, Venezuela). *Earth Planetary Sci. Lett.* 264, 438–451. doi: 10.1016/j.epsl.2007.10.002

McGee, D., Broecker, W. S., and Winckler, G. (2010). Gustiness: The driver of glacial dustiness? *Quaternary Sci. Rev.* 29, 2340–2350. doi: 10.1016/j.quascirev.2010.06.009

McGee, D., deMenocal, P. B., Winckler, G., Stuut, J. B. W., and Bradtmiller, L. I. (2013). The magnitude, timing and abruptness of changes in North African dust deposition over the last 20,000yr. *Earth Planetary Sci. Lett.* 371-372, 163–176. doi: 10.1016/j.epsl.2013.03.054

Meskhidze, N., Völker, C., Al-Abadleh, H. A., Barbeau, K., Bressac, M., Buck, C., et al. (2019). Perspective on identifying and characterizing the processes controlling iron speciation and residence time at the atmosphere-ocean interface. *Mar. Chem.* 217, 103704. doi: 10.1016/j.marchem.2019.103704

Montgomery, D. C., Runger, G. C., and Hubele, N. F. (2009). *Engineering statistics* (Wiley, New York, NY: John Wiley & Sons).

Moore, C. M., Mills, M. M., Achterberg, E. P., Geider, R. J., LaRoche, J., Lucas, M. I., et al. (2009). Large-scale distribution of Atlantic nitrogen fixation controlled by iron availability. *Nat. Geosci.* 2, 867–871. doi: 10.1038/ngeo667

Muhs, D. R., Budahn, J. R., Prospero, J. M., and Carey, S. N. (2007). Geochemical evidence for African dust inputs to soils of western Atlantic islands: Barbados, the Bahamas, and Florida. *J. Geophysical Res.* 112(F2). doi: 10.1029/2005JF000445

Muhs, D. R., Budahn, J. R., Prospero, J. M., Skipp, G., and Herwitz, S. R. (2012). Soil genesis on the island of Bermuda in the Quaternary: The importance of African dust transport and deposition. *J. Geophysical Res.: Earth Surface* 117(F3). doi: 10.1029/2012JF002366

Oakes, M., Ingall, E., Lai, B., Shafer, M., Hays, M., Liu, Z., et al. (2012). Iron solubility related to particle sulfur content in source emission and ambient fine particles. *Environ. Sci. Technol.* 46, 6637–6644. doi: 10.1021/es300701c

Ooki, A., Nishioka, J., Ono, T., and Noriki, S. (2009). Size dependence of iron solubility of Asian mineral dust particles. *J. Geophysical Research-Atmospheres* 114 (D3). doi: 10.1029/2008JD010804

Owens, J. D., Lyons, T. W., Li, X. N., Macleod, K. G., Gordon, G., Kuypers, M. M. M., et al. (2012). Iron isotope and trace metal records of iron cycling in the proto-North Atlantic during the Cenomanian-Turonian oceanic anoxic event (OAE-2). *Paleoceanography* 27(3). doi: 10.1029/2012PA002328

Poulton, S. W., and Canfield, D. E. (2005). Development of a sequential extraction procedure for iron: implications for iron partitioning in continentally derived particulates. *Chem. Geol.* 214, 209–221. doi: 10.1016/j.chemgeo.2004.09.003

Poulton, S. W., and Raiswell, R. (2005). Chemical and physical characteristics of iron oxides in riverine and glacial meltwater sediments. *Chem. Geol.* 218, 203–221. doi: 10.1016/j.chemgeo.2005.01.007

Prospero, J. M., and Mayol-Bracero, O. L. (2013). Understanding the transport and impact of African dust on the Caribbean basin. *Bull. Am. Meteorological Soc.* 94, 1329–1337. doi: 10.1175/BAMS-D-12-00142.1

Pye, K. (1989). "Processes of fine particle formation, dust source regions, and climatic changes," in *Paleoclimatology and Paleometeorology: Modern and Past Patterns of Global Atmospheric Transport* (Springer), 3–30.

Raiswell, R., and Canfield, D. E. (2012). The iron biogeochemical cycle past and present. *Geochemical Perspect.* 1, 1–220. doi: 10.7185/geochempersp.1.1

Raiswell, R., Hardisty, D. S., Lyons, T. W., Canfield, D. E., Owens, J. D., Planavsky, N. J., et al. (2018a). The iron paleoredox proxies: A guide to the pitfalls, problems and proper practice. *Am. J. Sci.* 318, 491–526. doi: 10.2475/05.2018.03

Raiswell, R., Hawkings, J., Elsenousy, A., Death, R., Tranter, M., and Wadham, J. (2018b). Iron in glacial systems: Speciation, reactivity, freezing behaviour and alteration during transport. *Front. Earth Sci.* 6, 222. doi: 10.3389/feart.2018.00222

Ridgwell, A., and Hargreaves, J. (2007). Regulation of atmospheric $CO_{2\ by}$ deep-sea sediments in an Earth system model. *Global Biogeochemical Cycles* 21(2). doi: 10.1029/2006GB002764

Sardar Abadi, M., Owens, J. D., Liu, X., Them, T. R., Cui, X., Heavens, N. G., et al. (2020). Atmospheric dust stimulated marine primary productivity during Earth's penultimate icehouse. *Geology.* 48, 247-251. doi: 10.1130/G46977.1

Schwertmann, U., Stanjek, H., and Becher, H.-H. (2004). Long-term in *vitro* transformation of 2-line ferrihydrite to goethite/hematite at 4, 10, 15 and 25 C. *Clay Minerals* 39, 433–438. doi: 10.1180/0009855043940145

Shaked, Y., and Lis, H. (2012). Disassembling iron availability to phytoplankton. *Front. microbiol.* 3, 123. doi: 10.3389/fmicb.2012.00123

Shi, Z. B., Krom, M. D., Bonneville, S., Baker, A. R., Jickells, T. D., and Benning, L. G. (2009). Formation of iron nanoparticles and increase in iron reactivity in mineral dust during simulated cloud processing. *Environ. Sci. Technol.* 43, 6592–6596. doi: 10.1021/es901294g

Shinn, E. A., Smith, G. W., Prospero, J. M., Betzer, P., Hayes, M. L., Garrison, V., et al. (2000). African dust and the demise of Caribbean coral reefs. *Geophysical Res. Lett.* 27, 3029–3032. doi: 10.1029/2000GL011599

Shoenfelt, E. M., Sun, J., Winckler, G., Kaplan, M. R., Borunda, A. L., Farrell, K. R., et al. (2017). High particulate iron (II) content in glacially sourced dusts enhances productivity of a model diatom. *Sci. Adv.* 3, e1700314. doi: 10.1126/sciadv.1700314

Shoenfelt, E. M., Winckler, G., Lamy, F., Anderson, R. F., and Bostick, B. C. (2018). Highly bioavailable dust-borne iron delivered to the Southern Ocean during glacial periods. *Proc. Natl. Acad. Sci.* 115, 11180–11185. doi: 10.1073/pnas.1809755115

Skonieczny, C., McGee, D., Winckler, G., Bory, A., Bradtmiller, L., Kinsley, C., et al. (2019). Monsoon-driven Saharan dust variability over the past 240,000 years. *Sci. Adv.* 5, eaav1887. doi: 10.1126/sciadv.aav1887

Skulan, J. L., Beard, B. L., and Johnson, C. M. (2002). Kinetic and equilibrium Fe isotope fractionation between aqueous Fe(III) and hematite. *Geochimica Cosmochimica Acta* 66, 2995–3015. doi: 10.1016/S0016-7037(02)00902-X

Spokes, L. J., Jickells, T. D., and Lim, B. (1994). Solubilisation of aerosol trace metals by cloud processing: A laboratory study. *Geochimica Cosmochimica Acta* 58, 3281–3287. doi: 10.1016/0016-7037(94)90056-6

Sur, S., Owens, J. D., Soreghan, G. S., Lyons, T. W., Raiswell, R., Heavens, N. G., et al. (2015). Extreme eolian delivery of reactive iron to late Paleozoic icehouse seas. *Geology* 43, 1099–1102. doi: 10.1130/G37226.1

Swart, P. K., Oehlert, A., Mackenzie, G., Eberli, G. P., and Reijmer, J. (2014). The fertilization of the Bahamas by Saharan dust: A trigger for carbonate precipitation? *Geology* 42, 671–674. doi: 10.1130/G35744.1

Thöle, L. M., Amsler, H. E., Moretti, S., Auderset, A., Gilgannon, J., Lippold, J., et al. (2019). Glacial-interglacial dust and export production records from the Southern Indian Ocean. *Earth planetary Sci. Lett.* 525, 115716. doi: 10.1016/j.epsl.2019.115716

Tiedemann, R., Sarnthein, M., and Stein, R. (1989). Climatic changes in the western Sahara: Aeolo-marine sediment record of the last 8 million years (sites 657-661). *Proc. ocean drilling program Sci. results* 108, 241-277. College Station, Tex.: Ocean Drilling Program.

Trapp, J. M., Millero, F. J., and Prospero, J. M. (2010). Trends in the solubility of iron in dust-dominated aerosols in the equatorial Atlantic trade winds: Importance of iron speciation and sources. *Geochem. Geophys. Geosystems* 11(3). doi: 10.1029/2009GC002651

Viollier, E., Inglett, P., Hunter, K., Roychoudhury, A., and Van Cappellen, P. (2000). The ferrozine method revisited: Fe (II)/Fe (III) determination in natural waters. *Appl. geochemistry* 15, 785–790. doi: 10.1016/S0883-2927(99)00097-9

Waeles, M., Baker, A. R., Jickells, T., and Hoogewerff, J. (2007). Global dust teleconnections: aerosol iron solubility and stable isotope composition. *Environ. Chem.* 4, 233–237. doi: 10.1071/EN07013

Ward, B. A., Wilson, J. D., Death, R. M., Monteiro, F. M., Yool, A., and Ridgwell, A. (2018). EcoGEnIE 1.0: plankton ecology in the cGEnIE Earth system model. *Geoscientific Model. Dev.* 11, 4241–4267. doi: 10.5194/gmd-11-4241-2018

Wells, M. L., Zorkin, N. G., and Lewis, A. (1983). The role of colloid chemistry in providing a source of iron to phytoplankton. *J. Mar. Res.* 41, 731–746. doi: 10.1357/002224083788520478

Yarincik, K., Murray, R., and Peterson, L. (2000). Climatically sensitive eolian and hemipelagic deposition in the Cariaco Basin, Venezuela, over the past 578,000 years: Results from Al/Ti and K/Al. *Paleoceanography* 15, 210–228. doi: 10.1029/1999PA900048

Yu, H., Chin, M., Yuan, T., Bian, H., Remer, L. A., Prospero, J. M., et al. (2015). The fertilizing role of African dust in the Amazon rainforest: A first multiyear assessment based on data from Cloud-Aerosol Lidar and Infrared Pathfinder Satellite Observations. *Geophysical Res. Lett.* 42, 1984–1991. doi: 10.1002/2015GL063040

Zhang, Y., Mahowald, N., Scanza, R., Journet, E., Desboeufs, K., Albani, S., et al. (2015). Modeling the global emission, transport and deposition of trace elements associated with mineral dust. *Biogeosciences.* 12, 5771-5792. doi: 10.5194/bgd-11-17491-2014